•水利与土木工程•

**DOI:**10.12454/j.jsuese.202400061

本刊网刊

# 黄河下游冲积地层旋挖变径桩竖向承载性能研究

邵广彪[1,2]，申佳佳[3]，焦伟杰[3]，韩健勇[1,2*]，刘学林[4]，陈济遥[1]

(1.山东建筑大学 土木工程学院，山东 济南 250101；2.山东建筑大学工程鉴定加固研究院有限公司，山东 济南 250013；
3.济南国际机场建设有限公司，山东 济南 250107；4.中国建筑设计研究院有限公司，北京 100032)

**摘　要：**黄河下游冲积平原为典型新近沉积地层，在该地层下采用旋挖工艺会提高变径桩的施工效率，但目前针对旋挖变径桩在典型黄河冲积粉黏互层的力学性能研究尚不深入。为探究该地层旋挖变径桩竖向抗压承载性能，本文开展了现场静载试验、单桩承载数值计算和极限承载力理论分析研究。结果显示：桩体达到承载力极限时，呈现出缓变破坏特征，桩侧摩阻和端阻的发挥是异步的，桩身上部摩阻力先于下部发挥到极限，且侧摩阻要先于端阻发挥完成；桩身下部扩径可增加端阻承载，降低桩体沉降量，延缓桩身变形，使桩侧摩阻得到进一步发挥；相同直径下，变径桩受压时桩身压缩量在总沉降量中的占比小于等直径桩，桩身变形程度更小，侧摩阻发挥更完全；变径桩桩周土塑性区同时于桩顶和扩径部位发生塑性形变，塑性区随荷载增大自上而下拓展，直至桩端塑性区加大而破坏，其主要影响桩周 2 m范围内的土体，等直径桩塑性破坏范围远超变径桩；数值及理论计算表明，变径桩的极限承载力可超出规范计算承载力极限 10%～20%。总体来看，黄河下游冲积地层变径桩呈现摩擦端承桩破坏特征，并验证了变径桩承载力的计算方法，研究成果可对黄河下游冲积地层该类桩基设计及理论计算提供参考。

**关键词：**黄河冲积地层；变径桩；静载试验；受力性能；极限承载力；数值模拟

**中图分类号：**TU 473.1　　**文献标志码：**A　　**文章编号：**2096-3246(2026)02-0179-12

变径桩于20世纪60年代在中国开始使用，并随着施工工艺和机械的发展在工程中的应用越来越广泛，其扩径设计增大了桩土接触面积，较常规等直径桩相比可满足重要建筑物更为严格的沉降要求。目前，已有学者[1−3]通过静载试验验证了不同类型变径桩承载性能优于等直径桩。Ilamparuthi 等[4]通过在砂土中开展扩底桩抗拔试验，提出预测扩底桩抗拔承载力的经验方法。刘伟平等[5]通过静载试验研究了挖孔变径桩的承载特性和荷载传递机理。刘双[6]对大直径扩底桩的荷载传递规律进行了试验研究，将不同方式计算出的桩极限荷载与试验数据进行对比，发现利用沉降拐点计算极限荷载的方法结果较小。马运锋[7]利用试验和模拟方法对变径桩在土性良好和不良地区的抗压承载性能进行了对比，发现良好地层能有效增大端承效应。王卫东等[8]在软土地区对桩端扩大头的极限抗压承载性能开展了试验研究，发现桩端扩大头极限承载力实测结果大于规范计算结果。Majumder 等[9]估算了非均质黏土中扩孔桩的承载力，详细研究了长径比、扩径位置和扩径角等参数对桩体承载力的影响。Peter 等[10]分析了扩底桩在不同土层中的承载特性，对比了其在不同土质条件下的承载性能差异。此外，在实际工程或试验中难以测定变径桩的数据可以通过数值模拟进行补充研究[11−13]。

黄河下游冲积平原多为第四系地层，地层结构以黏土、粉土和粉砂为主[14−16]，地基土的承载力较低，具有其特有的互层结构。董三升[17]、董志强[18]等通过静载试验与数值模拟等方法得到了黄河中下游平原等直径单桩的承载力及沉降规律，发现灌注扩孔桩在施工与造价上具有优势。随着国家推动黄河流域高质量发展战略的实施，变径桩成为了对沉降要求严格的重要工程的优选，其中旋挖施工变径桩具有速度快、污染少、设备充足等优点，但目前针对在黄河下游冲积

**收稿日期：**2024－01－23　　**修回日期：**2024－05－05　　**网络出版日期：**2024－06－04

**基金项目：**国家自然科学基金项目(42172310)；国家外专项目(G2022023020L)；甘肃省重点研发计划项目(22YF7FH224)

**作者简介：**邵广彪(1978—)，男，教授，博士．研究方向：城市复杂环境岩土力学及地下工程防灾减灾．E-mail：Shaogb@sdjzu.edu.cn

* **通信作者：**韩健勇，副教授，E-mail：hanlwb@163.com

地层条件下变径桩的相关研究还不充分，仍需深入探究变径桩的竖向承载性能。

本文通过现场静载试验和数值模拟对旋挖变径桩的单桩抗压性能沉降规律进行研究，探讨变径桩的受力机理与荷载传递特征，研究变径桩的力学性能，以期为该地区变径桩的设计及理论计算提供参考和借鉴。

## 1 现场试验

试验依托济南遥墙机场二期改扩建工程，场地地处黄河冲积平原地貌单元，地势整体平缓。场地内上部地层为黄河冲积漫滩相新近堆积土，以黏性土、粉土为主；下部地层为第四系全新统冲积土及第四系上更新统冲洪积土，以黏性土为主；地表为人工填土。场地地层物理力学参数见表1。

### 1.1 试验桩体参数

抗压静载试验共有6根试验桩，桩径分800 mm和1 000 mm两种类型，各3根。变径桩的扩径部分最大尺寸是基础桩径的两倍，每根试验桩间距为9 m，桩位布置如图1所示。

试验桩工艺为旋挖成孔，旋挖到底后更换扩孔钻头，在距桩底0.6 m处进行扩孔。扩孔钻头及扩孔形状如图2所示，该变径做法可有效提高桩端接触面积和端阻承载力。

未确定的静载试验加载值，根据《建筑桩基技术规范》[19]对变径桩单桩极限承载力标准值$Q_{uk}$进行估算：

表1 试验场地地层物理力学参数

Tab. 1 Physical and mechanical parameters of stratum in test site

| 地层编号 | 土层类型 | 重度/(kN·m$^{-3}$) | 压缩模量/MPa | 黏聚力/kPa | 内摩擦角/(°) | 侧阻力标准值/kPa |
|---|---|---|---|---|---|---|
| ① | 素填土 | 19.0 | — | 10.0 | 12.0 | 20～28 |
| ② | 粉土 | 18.9 | 9.56 | 15.0 | 21.7 | 42～62 |
| ③ | 粉质黏土 | 18.3 | 4.78 | 24.8 | 10.3 | 53～68 |
| ④ | 粉土 | 19.2 | 9.46 | 15.6 | 19.9 | 42～62 |
| ⑤ | 粉质黏土 | 19.2 | 4.96 | 27.8 | 13.5 | 53～68 |
| ⑥ | 粉土 | 19.6 | 10.03 | 18.8 | 29.6 | 42～62 |
| ⑦ | 粉质黏土 | 19.9 | 5.29 | 29.4 | 13.7 | 68～96 |
| ⑧ | 粉土 | 20.0 | 9.55 | 15.8 | 21.6 | 62～82 |
| ⑨ | 粉质黏土 | 19.8 | 6.24 | 27.2 | 13.2 | 84～96 |
| ⑩ | 粉土 | 19.9 | 8.23 | 19.4 | 27.8 | 62～82 |
| ⑪ | 粉质黏土 | 19.5 | 6.80 | 35.5 | 14.9 | 84～96 |
| ⑫ | 黏土 | 19.4 | 6.36 | 33.3 | 11.9 | 84～96 |
| ⑬ | 粉质黏土 | 19.5 | 6.37 | 34.1 | 13.0 | 84～96 |
| ⑭ | 黏土 | 19.1 | 6.66 | 40.3 | 14.6 | 96～102 |
| ⑮ | 粉质黏土 | 19.4 | 6.76 | 43.1 | 15.2 | 96～102 |
| ⑯ | 黏土 | 19.3 | 7.23 | 47.0 | 16.2 | 96～102 |
| ⑰ | 粉质黏土 | 19.4 | 7.04 | 38.8 | 15.5 | 96～102 |

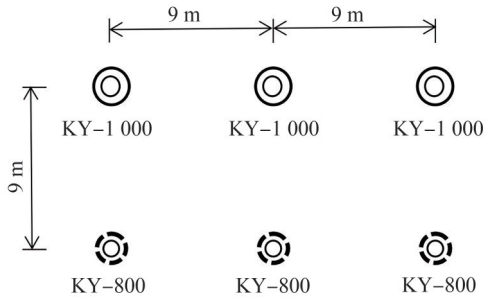


图1 试验桩桩位示意图

Fig. 1 Pile position diagram of test piles

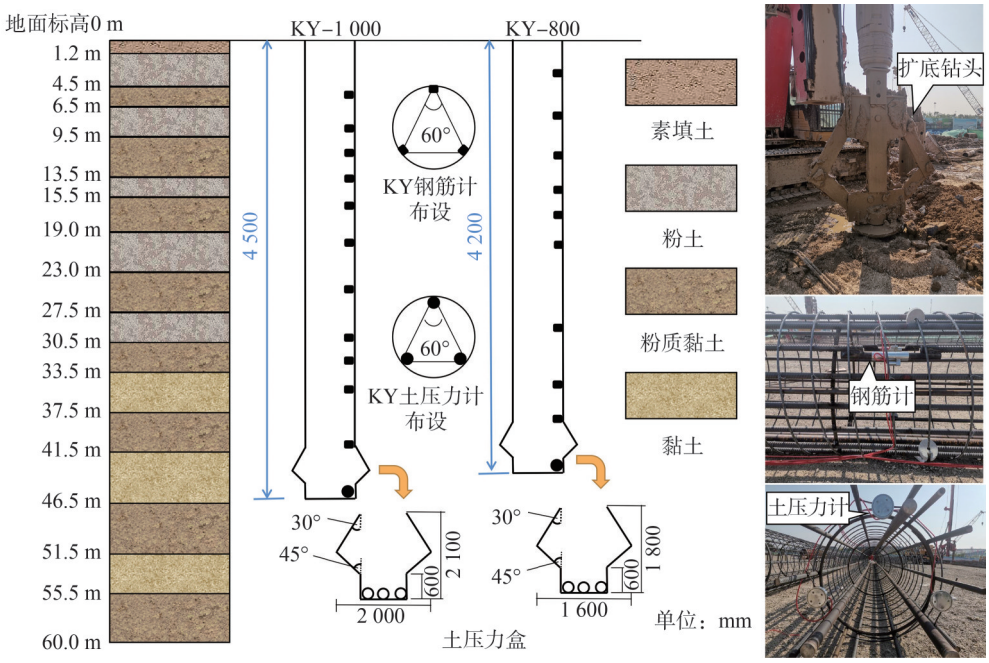


图2 试验桩体与扩孔钻头示意图

Fig. 2 Schematic diagram of the test pile and the reamer bit

$$Q_{uk}=Q_{sk}+Q_{pk}=u\sum q_{qik}l_i+\alpha q_{pk}A_p \quad (1)$$

式中，$Q_{sk}$、$Q_{pk}$为总极限侧阻力标准值和总极限端阻力标准值，$u$为桩身周长，$q_{sik}$为土的极限侧阻力，$l_i$为桩周第$i$层土层厚度，$\alpha$为桩端阻力修正系数，$q_{pk}$为端阻力标准值，$A_p$为桩底扩大端水平投影面积。试桩参数见表2。

**表2　试桩参数**

**Tab. 2　Test pile parameters**

| 桩型编号 | 桩径 $D$/mm | 桩长 $L$/m | 扩孔尺寸 $d$/mm | 极限承载力 $Q_{uk}$/kN | 最大加载量 $1.2Q_{uk}$/kN |
|---|---|---|---|---|---|
| KY–1 000 | 1 000 | 46 | 2 000 | 18 720 | 22 464 |
| KY–800 | 800 | 42 | 1 600 | 12 280 | 14 736 |

### 1.2　传感器安装

KY–1 000桩取12个横截面，在上层11个截面上安装钢筋计，在底部安装土压力盒；KY–800桩取10个横截面，在上层9个截面上安装钢筋计，在底部安装土压力盒。两类桩每个截面都布设3个钢筋计，成60°夹角分布。传感器布置如图2所示。

### 1.3　试验加载方法

根据《建筑基桩检测技术规范》[20]，试验加载采用慢速维持荷载法[21]，荷载分11级加载，第1级按$0.2Q_{uk}$加荷，后续每级增加$0.1Q_{uk}$，第9级达到$Q_{uk}$，待稳定后再继续施加第10级和第11级荷载。每级荷载施加稳定后，先测读竖向位移及传感器读数，再开始下一级加载，待达到最大荷载或桩顶总沉降量超过40 mm，终止加载；最后逐级卸荷到0。本次试验目的为探究试验桩极限承载力，故在桩体达到规范要求的终止条件后，仍继续加载直至第11级荷载。现场静载试验示意图如图3所示。

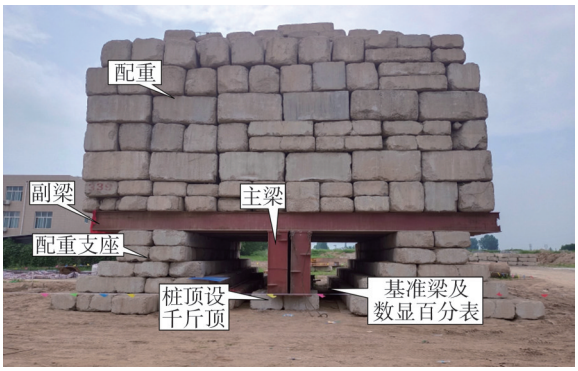


**图3　现场静载试验**

**Fig. 3　Field static load test**

## 2　试验结果

### 2.1　桩顶沉降位移

整理分析6根桩的试验数据，得到桩顶荷载$Q$与沉降量$S$的关系曲线，选取两类桩典型$Q$–$S$曲线，如图4所示。由图4可以看出：初始近似直线段部分表明桩身与周侧土结合良好，桩身与土体共同变形下沉，且KY–1 000桩表现更为明显；随后，$Q$–$S$曲线逐渐弯曲，表明桩侧摩阻力不断发挥到极限值，KY–1 000桩沉降较平缓；当加载值超过极限承载力时，沉降呈现加速状态，KY–800桩表现较为明显，加荷至$1.2Q_{uk}$时沉降增加了100%，而KY–1 000桩增加了约60%。总体上，变径桩$Q$–$S$曲线为典型的缓变型曲线，无明显转折，未产生剧烈沉降，尤其对于大直径变径桩，摩擦端承型桩的特征较为显著。

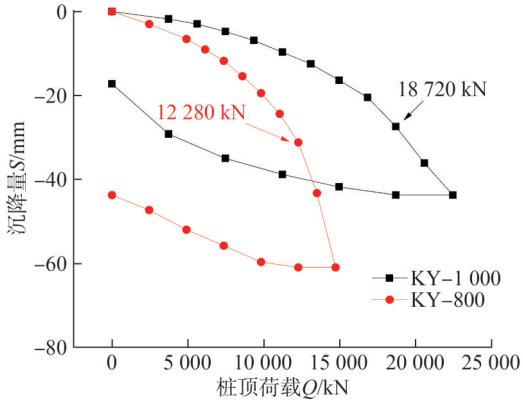


**图4　桩顶荷载–沉降曲线**

**Fig. 4　Load–settlement curves at the pile head**

由图4还可知：KY–1 000抗压桩加荷至$Q_{uk}$时的沉降量（27 mm）约为加荷至$1.2Q_{uk}$时的63%；KY–800抗压桩加荷至$Q_{uk}$时的沉降量（31 mm）约为加荷至$1.2Q_{uk}$时的51%。两桩卸载后有一定回弹，KY–1 000桩回弹量为24.5 mm，KY–800桩回弹量为17.2 mm，这是因为KY–1 000桩的桩身较长，桩身回弹量较大。由此可以看出变径旋挖桩的桩身变形性能良好。

### 2.2　桩身轴力分布

实测得到各级荷载下钢筋应变并计算得到桩身轴力，结果如图5所示。由图5可知：随着荷载的增加，桩身各截面轴力也随之增加；桩身轴力随深度的增加呈现出先增大后逐级减小的趋势。KY–800桩最大轴力首先位于7 m深度处，随荷载增加移至桩顶；KY–1 000桩最大轴力一直位于9 m深度处。分析其原因为上部地层软弱，安放配重堆载使桩周土产生负摩阻力。

由图5还可看出，在桩体最大承载范围内，两类桩地下15～35 m范围内的轴力变化有所不同。其中：KY–1 000桩轴力随埋深增加逐步减小；KY–800桩在约17 m处产生突变，这是由旋挖过程中产生塌孔导致该位置注浆后桩径增大所致。在地下20～35 m范围内，轴力无明显变化，这是由于本次试验桩为端承摩擦型桩，因此桩身轴力上段随深度减小，下部因桩土相对位移较小，桩侧摩阻发挥不完全，轴力变化较小。

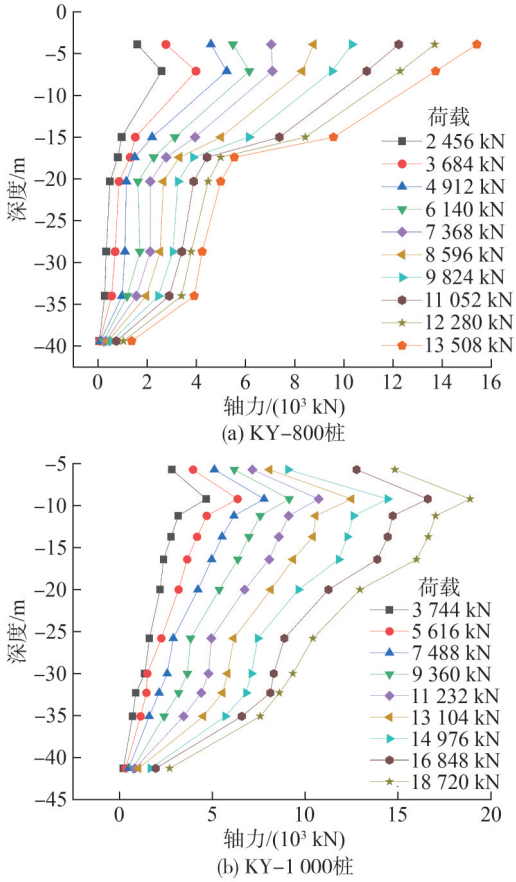


图5 桩身埋深–轴力曲线

**Fig. 5 Pile shaft burial depth–axial force curves**

### 2.3 桩侧摩阻力及桩端阻力分析

首先,假定在桩体深度范围内的每一分层土的侧摩阻力相同;再计算每一分层桩周侧平均摩阻力 $q_{si}$:

$$q_{si}=\frac{Q_i-Q_{i+1}}{A_j} \tag{2}$$

式中,$Q_i$为第$i$个断面的轴力,$A_j$为第$j$分层桩侧面积。

计算得出KY–800桩与KY–1 000桩在不同荷载作用下桩周平均侧摩阻力沿桩身的分布曲线,如图6所示。

由图6可知:桩周侧摩阻力为异步发挥,上部土层摩阻力要先于下部土层发挥作用;随着上部荷载增大,各层桩侧摩阻力逐步发挥。这是因为当极限摩阻力小的土层发挥到极限时,上部土层摩阻力已趋于稳定,但下部土层的摩阻力还未发挥完全。

图7为桩端阻力承载占比曲线(等直径桩数据来自本文依托项目同期试验)。由图7可知:变径桩桩端阻力承载占比曲线变化趋势呈现为先快速增加后增速变缓的趋势;等直径桩为前期增长较为缓慢,随后增长速度变快。其中:KY–1 000桩端阻力承载最终占比85.4%,KY–800桩端阻力承载最终占比为79.1%,但在相同荷载下,两类桩桩端承载占比大致相同,符合图4桩体沉降规律;等直径桩桩端承载占比明显小于

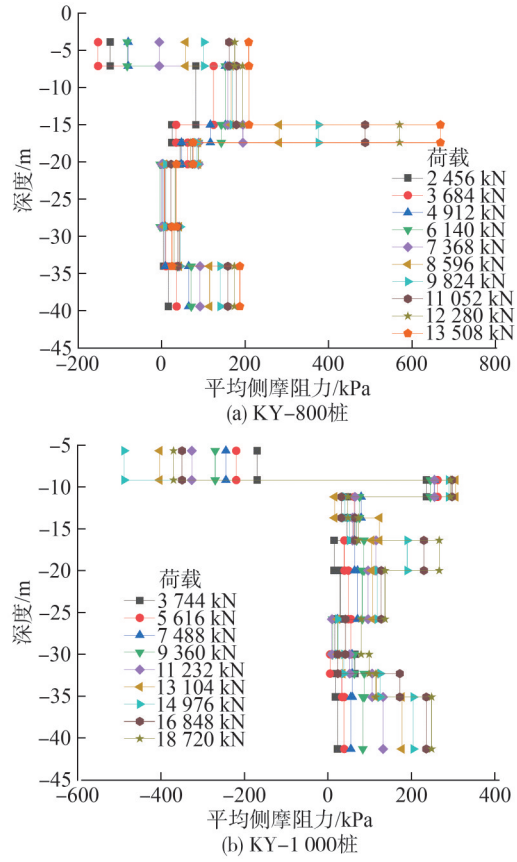


图6 桩周平均侧摩阻力分布曲线

**Fig. 6 Average lateral frictional resistance distribution curves around the pile**

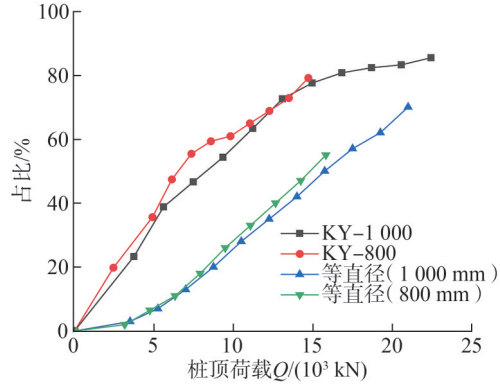


图7 桩端阻力承载占比

**Fig. 7 Proportion of pile tip resistance bearing capacity**

变径桩,说明变径桩的扩体构造有利于端阻的发挥。

综合图6、7可知,桩侧摩阻力和桩端阻力的发挥均为异步的过程,这意味着通过传统静力学经验公式,依照土层摩阻力平均值来计算桩周侧摩阻力并确定桩体承载力的方式并不完全适用于黄河冲积地层条件下的变径桩。对比桩身下部与15～20 m埋深范围桩侧摩阻力的变化(图6)可以发现,变径桩的扩大头部分因为分担了更多的荷载,减小了桩体沉降及桩身塑性变形,导致周边的桩土位移小于桩身其他位置的位移,进而影响桩侧摩阻力作用的发挥。

### 2.4　桩土相对位移

桩土相对位移量$\delta_i$的计算公式如下[22]：

$$\delta_i=\delta_0-\sum_{j=1}^{i}\frac{L_i}{2}\left(\varepsilon_j+\varepsilon_{j+1}\right) \tag{3}$$

式中，$L_i$为第$i$桩段的长度，$\varepsilon_j$为第$j$断面的实测应变，$\delta_0$为桩顶位移量。由式(3)计算得到不同深度地层桩周平均侧摩阻力与桩土相对位移关系曲线，如图8所示。

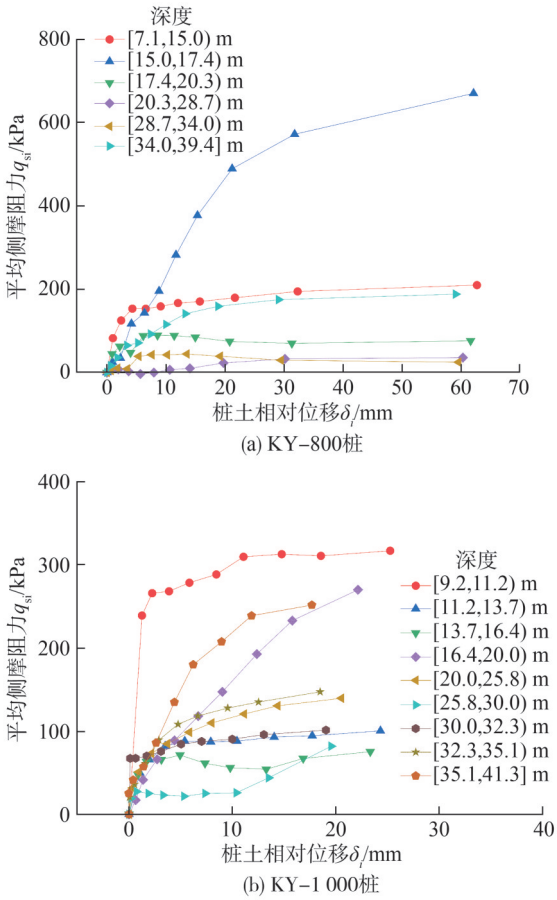


**图8　桩周平均侧摩阻力与桩土相对位移曲线**

**Fig. 8　Average lateral frictional resistance around the pile and the pile-soil relative displacement curves**

通过对试验数据分析可知，当黏土层中的桩体位移超过0.014$D$（$D$为桩径）、粉土层中桩体位移超过0.019$D$时，桩土间会发生滑移[23]，导致土体结构性破坏，影响侧摩阻力发挥。同时，随着上部荷载增加，滑移区开始向下扩展，直至延伸至桩端扩径处，此时桩身达到承载力极限，但因桩端存在，桩体不会直接损坏。与传统等直径桩相比，变径桩的扩径部分增大了桩土接触面积，在相同桩长情况下可使桩周侧摩阻力更好地发挥，从而提供更大的承载力。

## 3　数值模拟

为进一步研究黄河下游冲积地层旋挖变径桩的单桩承载特性与破坏特征，利用Plaxis 3D有限元软件对变径桩和同尺寸等直径桩进行竖向加载模拟。

### 3.1　模型建立

参考场地地勘报告，黄河冲积地层土体本构模型采用H–S模型[24–26]；桩体参数采用试验桩参数，重度$\gamma$=25 kN/m$^3$，弹性模量$E$=32.5 GPa，泊松比$\mu$=0.15；桩身采用弹性模型；桩土界面强度折减系数取0.6，桩体和土体均采用实体单元模拟，桩身尤其是扩径部分网格加密，据此建立三维计算模型。模型平面大小取50 m×50 m，地基深度取60 m。数值模型如图9所示。

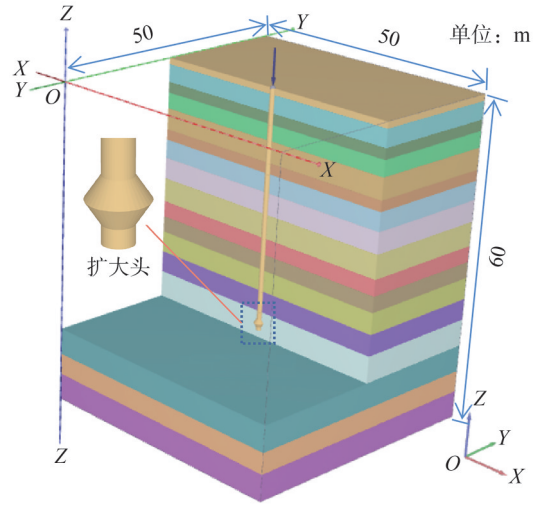


**图9　数值模型**

**Fig. 9　Numerical model**

### 3.2　模型验证

为验证数值模型的准确性，利用现场试验结果对数值模型关键参数进行标定。对现场试验桩按照实际加载工况进行模拟计算，编号MKY–1 000和MKY–800分别代表直径为1 000 mm桩和800 mm桩。桩顶荷载–位移计算与实测结果对比如图10所示。由图10可知：各加载工况下，两者相差较小，1 000 mm桩最大沉降两者相差4.7 mm，800 mm桩最大沉降相差3.1 mm；模拟曲线变化更为平滑，但整体变化趋势与实测曲线大

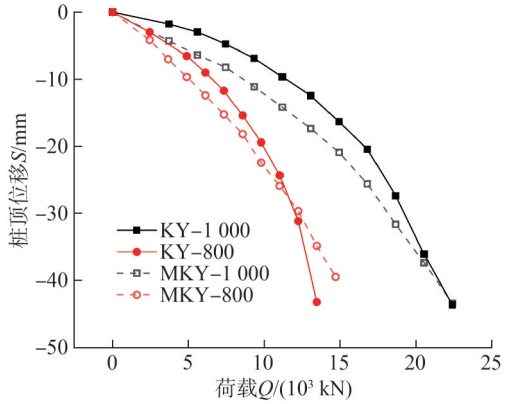


**图10　桩顶荷载–位移计算与实测结果对比**

**Fig. 10　Comparison between simulation and test results of pile head load–displacement**

致相同，可见模型较准确，满足进一步研究的要求。

### 3.3 扩径影响分析

建立等直径桩（编号MKY–DZJ）的数值模型，除无变径段外，其余参数同变径桩。数值模拟得到各类型桩极限承载力值：MKY–DZJ（800 mm桩）为13 508 kN，MKY–800为14 736 kN，MKY–DZJ（1 000 mm桩）为20 592 kN，MKY–1 000为22 464 kN。由模拟结果可知：同参数条件下，变径桩极限承载力超出等直径桩约1/10；在模拟沉降与实测沉降差距较小情况下，数值模拟得到的极限承载力值要高于规范计算得出的极限承载力值。

图11为桩身压缩量$S_S$占桩顶沉降$S$百分比曲线（桩身压缩量为桩顶与桩底沉降量之差）。由图11可知：桩径越大，$S_S$的占比越小；等直径桩受压过程中的

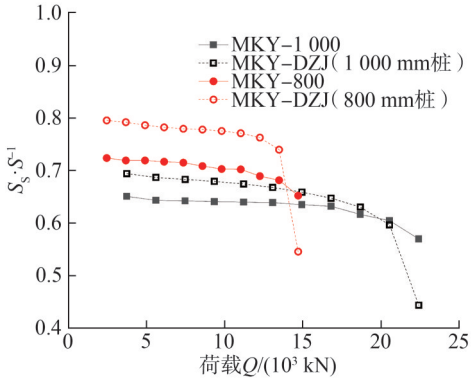


**图11 各级荷载下桩身变形量占桩顶沉降百分比曲线**

**Fig. 11 Curves of pile deformation as a percentage of pile top settlement under different levels of load**

$S_S$的占比明显超过同桩径下的变径桩；在达到极限荷载后，等直径桩桩端产生大位移，桩身压缩量占桩顶沉降量比例明显下降，变径桩桩身压缩量依然稳定。

从整体看，在黄河冲积平原地层条件下，桩径1 m及以下的变径桩的桩身压缩量超过桩顶沉降量的60%，所占比例较大，故应将该类桩视为非刚性桩来考虑。在进行沉降计算时，要考虑到当变径桩桩顶沉降达到预期控制值时，其桩端阻力尚未充分发挥，从而选取合适的桩长及长径比[27–30]。

### 3.4 桩周土屈服演化特性

选取MKY–1 000和MKY–DZJ（1 000 mm桩）两桩的计算结果，对比4个加载阶段的桩周土塑性区分布，如图12所示。由图12可知：在加载初期，桩周土的塑性变形区范围较小，仅在桩端和桩上侧土体产生小部分塑性变形；随着上部荷载的增大，桩侧摩阻力逐渐开始发挥，塑性区随之扩大，从桩身上部逐渐延伸至中下部；当下部土层的侧摩阻力基本发挥完全，端阻发挥作用时，端部塑性区向周边扩展，桩周土产生较大塑性变形。

由图12可知，两类桩的桩周土塑性区在前两个加载阶段基本一致，主要区别在于：达到图12（c）所示阶段时，等直径桩塑性区已经明显超过变径桩；达到图12（d）所示阶段时，等直径桩超过承载力极限，连同桩周土已经完全塑性破坏，表现为塑性区发展到模型边界处，而变径桩桩周土塑性区还能保持在一定范围内（软件仅显示当前施工步新增塑性区）。

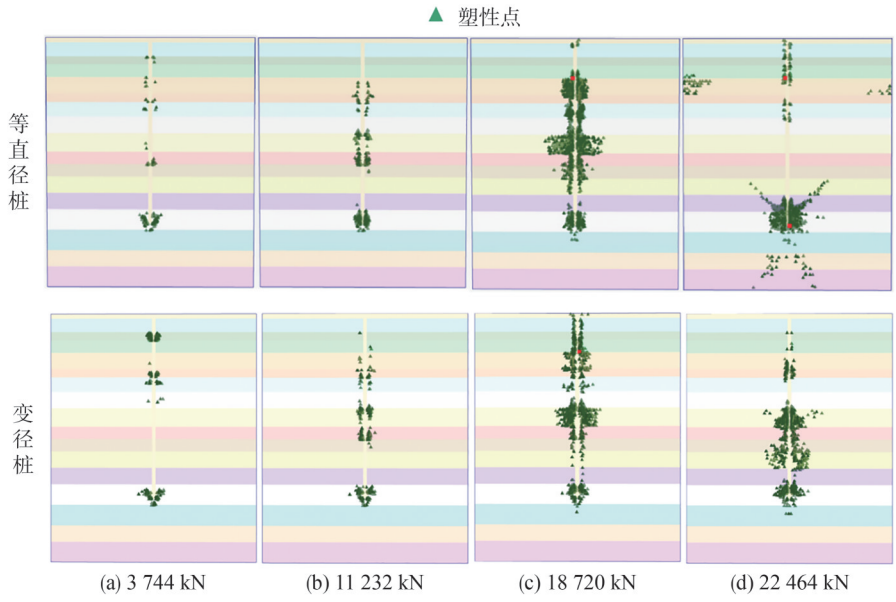


**图12 不同荷载下等直径桩和变径桩周土塑性区分布**

**Fig. 12 Plastic zones distribution of soil around equal diameter pile and variable diameter pile under different loads**

### 3.5 桩周土沉降变化规律

图13为变径桩和等直径桩在极限荷载下不同深度桩周土的沉降变化曲线。由图13（a）可知：桩顶地表最大沉降达35 mm，而桩端处仅12 mm。距离变径桩

2 m范围内土体沉降变化最为明显，为主要影响区；至10 m处，土体沉降随距离增大逐渐减小，为次要影响区；10 m以外范围曲线基本不再变化，为无影响区。

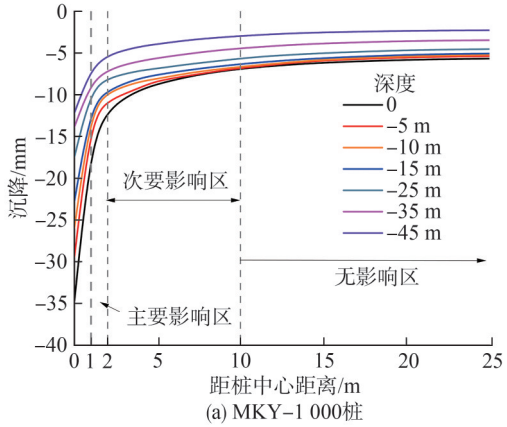

(a) MKY−1 000桩

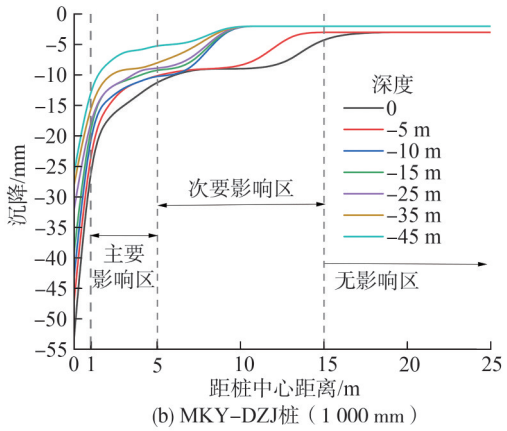

(b) MKY−DZJ桩（1 000 mm）

**图13　在不同深度处等直径桩和变径桩桩周土沉降曲线**

**Fig. 13　Soil settlement curves around the equal diameter pile and the variable diameter pile at different depths**

由图13(b)可知：桩顶地表最大沉降达53 mm，桩端处为23 mm。等直径桩在主要影响区（5 m范围内）的沉降量超出变径桩约1/3；在地下10 m范围内的沉降次要影响区扩大到距桩中心15 m水平范围。此外，次要影响区的沉降变化并不平缓，这是因为等直径桩作为摩擦桩，桩顶沉降量大，桩身变形也超过变径桩（图11），桩周土会有向桩体移动的趋势，这就导致0～5 m深度土层的沉降影响范围更大，与变径桩形成鲜明对比。

由此可见，变径桩能更好地发挥桩端阻力和桩侧阻力，有效减小桩周土的沉降量和影响范围。

## 4　变径桩极限承载力计算

由试验与模拟结果可知，以$Q$–$S$曲线拐点作为变径桩极限承载力具有一定的局限性，这是由于该方法受试验条件影响较大，同时也存在拐点并不明显而无法准确判断极限承载力的问题。基于此，需要通过其他方法对变径桩极限承载力进行分析[6]。

高盟等[31]提出变径桩桩端沉降$S'$修正公式为：

$$S'=\frac{rI_{\mathrm{p}}q}{E_0} \tag{4}$$

$$q=\left(Q+G_{\mathrm{fk}}\right)/A_{\mathrm{p}}-\left(\pi Dq_{\mathrm{sk}}L/A_{\mathrm{p}}\right)-\gamma_0 l_{\mathrm{m}} \tag{5}$$

式(4)、(5)中：$r$为扩大端半径；$I_{\mathrm{p}}$为变径桩沉降影响系数，本文取0.565；$q$为桩端均布荷载；$E_0$为桩端持力层土体变形模量；$G_{\mathrm{fk}}$为变径桩自重标准值；$q_{\mathrm{sk}}$为扩大端变截面以上桩长范围内按土层厚度计算的加权平均极限侧摩阻力标准值；$L$为扩大端变截面以上桩身长度；$\gamma_0$为桩入土深度范围内土层重度的加权平均值；$l_{\mathrm{m}}$为桩入土深度。

同时，考虑到桩端土的变形，对变径桩的沉降计算进行修正，变形模量与室内压缩模量间的关系为[32]：

$$E_0=\beta_0 E_{\mathrm{s1-2}} \tag{6}$$

式中：$\beta_0$为桩端土体计算变形模量修正系数，根据内插法取1.174；$E_{\mathrm{s1-2}}$为桩端持力层土体压缩模量，本文取9.03 MPa。

将桩体视为刚性桩，通过式(4)～(6)计算出桩端（即桩顶）沉降值，并与桩顶沉降实测值进行对比，结果见表3。

**表3　桩顶沉降的计算值与实测值的对比**

**Tab. 3　Comparison between calculated and measured of pile head settlements**

| 变径桩直径/mm | 荷载/kN | 每级实测值/mm | 每级计算值/mm | 误差/% |
|---|---|---|---|---|
| 1 000 | 3 744 | 1.79 | 1.54 | 13.88 |
| | 5 616 | 1.19 | 1.02 | 14.48 |
| | 7 488 | 1.80 | 1.55 | 13.86 |
| | 9 360 | 2.13 | 1.84 | 13.53 |
| | 11 232 | 2.77 | 2.41 | 12.90 |
| | 13 104 | 2.79 | 2.43 | 12.88 |
| | 14 976 | 3.89 | 3.43 | 11.78 |
| | 16 848 | 4.08 | 3.61 | 11.59 |
| | 18 720 | 6.94 | 6.33 | 8.73 |
| | 20 592 | 8.70 | 8.10 | 6.97 |
| | 22 464 | 7.57 | 6.96 | 8.10 |
| 800 | 2 456 | 2.98 | 2.80 | 6.14 |
| | 4 912 | 3.57 | 3.37 | 5.55 |
| | 6 140 | 2.48 | 2.32 | 6.64 |
| | 7 368 | 2.71 | 2.54 | 6.41 |
| | 8 596 | 3.65 | 3.45 | 5.47 |
| | 9 824 | 4.03 | 3.82 | 5.09 |
| | 11 052 | 4.91 | 4.70 | 4.21 |
| | 12 280 | 6.82 | 6.67 | 2.30 |
| | 13 508 | 12.05 | 12.40 | 2.93 |
| | 14 736 | 17.67 | 16.77 | 5.14 |

由表3可知：直径1 000 mm变径桩的计算沉降值较实测值略小，误差约为6%～15%；直径800 mm变径桩的计算值和实测值数据相近，误差约2%～7%。

整体来看，计算结果具有可信度。变径桩桩顶沉

降实测值、模拟值与计算值 $Q$–$S$ 对比曲线如图 14 所示。

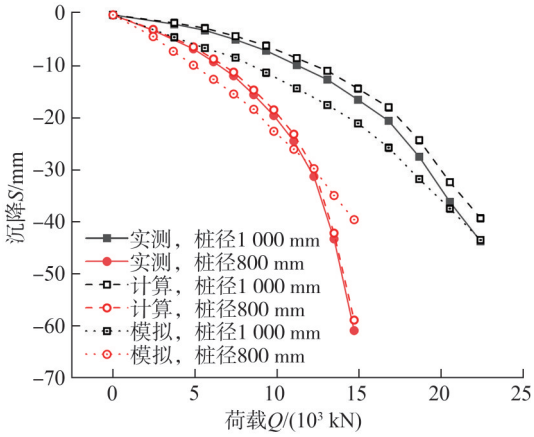


**图 14　实测值、模拟值与计算值 $Q$–$S$ 对比曲线**

**Fig. 14　$Q$–$S$ comparison curves of measured value, simulated value and calculated value**

Van[33]提出通过静载试验结果计算变径桩极限承载力的方式，即利用荷载 $Q$ 与桩顶沉降 $S$ 表示极限荷载：

$$Q=Q_{\mathrm{u}}\left(1-\mathrm{e}^{aS}\right) \tag{7}$$

式中，$Q$ 为静载试验中的荷载，$Q_{\mathrm{u}}$ 为极限荷载，$a$ 为反映 $Q$–$S$ 曲线形状的系数。

如给定多个 $Q_{\mathrm{u}}$，则每个 $Q_{\mathrm{u}}$ 都可以得到一条 $Q$–$S$ 曲线，则最接近直线时所对应的 $Q_{\mathrm{u}}$ 即为变径桩的极限荷载。代入式(8)进行极限承载力计算，得到理论计算结果如图 15 所示。

$$S=\frac{1}{a}\ln\left(1-\frac{Q}{Q_{\mathrm{u}}}\right) \tag{8}$$

图 15 中：越接近直线表明越靠近极限承载力，故直径 1 000 mm 变径桩极限承载力值接近于 22 464 kN 而并非规范计算值的 18 720 kN；同样地，直径为 800 mm 变径桩极限承载力值接近于 14 736 kN，理论计算结果近似于数值模拟结果。由此可推断，变径桩在黄河冲积地层条件下，实际极限承载力值比通过现有规范计算所得到的极限承载力值高出 10%～20%。

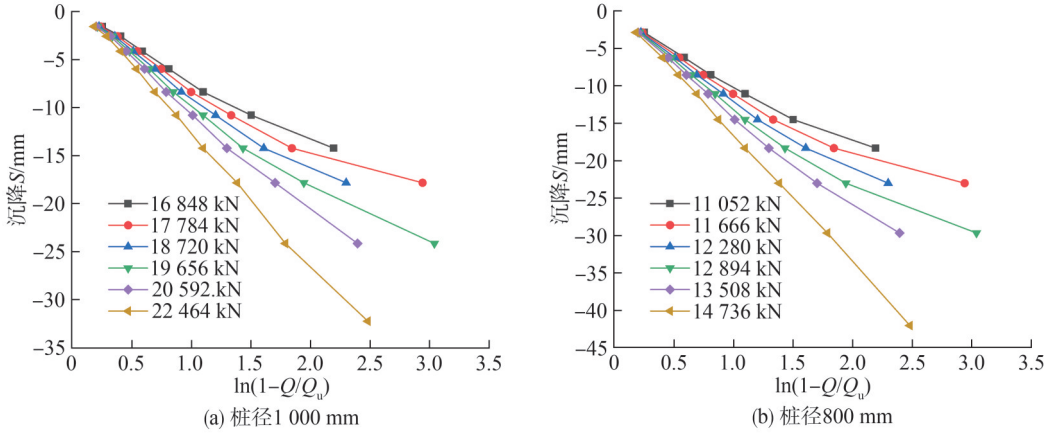


**图 15　极限承载力理论计算结果**

**Fig. 15　Theoretical calculation results of ultimate bearing capacity**

## 5　结　论

1）黄河下游冲积地层变径桩属典型摩擦端承型桩，桩体上部与下部侧摩阻的发挥存在异步特征。变径桩端阻能分担更多荷载，减小和延缓桩身沉降，使侧摩阻力更好发挥，从而整体上提高了单桩承载力。

2）变径桩桩身变形量小于等直径桩，接近非刚性桩，变径桩受压时，其桩侧土同时于桩顶和桩底扩大头发生塑性破坏，然后随荷载增大沿顶端向下延伸；变径桩对桩侧土的影响也小于等直径桩。

3）变径桩受压时，其桩侧土同时于桩顶和桩底扩大头发生塑性破坏，然后随荷载增大沿顶端向下延伸；不同于等直径桩，在达到极限荷载状态时，变径桩桩身缓慢破坏，对桩侧土的影响保持在约 2 m 范围内。

4）通过理论计算结合数值分析方法，得到本文试验变径桩的极限承载力超规范计算值约 10%～20%。

基于本次研究，加载初期变径桩的桩侧摩阻力变化规律同等直径桩基本一致，平均侧摩阻力呈近线性增长趋势，直至因变径扩体产生非线性、延缓的破坏而并非突然的脆性破坏。这一特性能有效降低实际工程中的安全风险，区别于等直径桩在黄河冲积地层中的受力特征，故可在类似试验设计中以此作为考察单桩极限承载能力的标志。

**参考文献：**

[1] Chen Jiegang.Load bearing mechanism and engineering application for high-pressure chemical belled pile[D]. Changsha:Hunan University,2009.[陈杰刚 . 高压旋喷扩底桩的承载机理及其工程应用[D].长沙：湖南大学，2009.]

[2] Hu Qinghong.Numerical analysis and experimental study

on the large diameter belled pile[D]. Hangzhou: Zhejiang University,2007.[胡庆红. 大直径扩底桩试验研究与数值分析[D]. 杭州:浙江大学,2007.]

[3] Ding Shengren. Experimental study on bearing capacity of large diameter hole-digging belled pile[D]. Xi'an: Changan University,2001.[丁胜仁. 大直径挖孔扩底桩承载性能试验研究[D]. 西安:长安大学,2001.]

[4] Ilamparuthi K,Dickin E A.Predictions of the uplift response of model belled piles in geogrid-cell-reinforced sand[J].Geotextiles and Geomembranes,2001,19(2):89–109.

[5] Liu Weiping, Fu Mingfu, Luo Xiaoyan, et al. Test investigation on characteristic of bearing capacity of large diameter manually excavated belled piles[J]. Journal of Nanchang University(Engineering & Technology),2006,28(1):60–63.[刘伟平,扶名福,罗小艳,等. 大直径挖孔扩底桩承载特性试验研究[J]. 南昌大学学报(工科版),2006,28(1):60–63.]

[6] Liu Shuang. Study on mechanical properties and key construction technology of large-diameter belled pile with enlarged bottom[D].Harbin:Northeast Forestry University, 2022.[刘双. 大直径扩底桩受力性能及施工关键技术研究[D]. 哈尔滨:东北林业大学,2022.]

[7] Ma Yunfeng. Study on bearing capacity of expanded pile in Changchun mudstone area[D]. Baotou: Inner Mongolia University of Science & Technology,2019.[马运锋. 长春泥岩地区扩底桩承载性能研究[D]. 包头:内蒙古科技大学,2019.]

[8] Wang Weidong, Wang Meng, Wu Jiangbin. Field study on the ultimate bearing capacity of enlarged grout base of pre-bored grouted planted pile[J]. Rock and Soil Mechanics,2023,44(11):3091–3098.[王卫东,王萌,吴江斌. 静钻根植桩扩底桩端极限承载性能的试验研究[J]. 岩土力学,2023,44(11):3091–3098.]

[9] Majumder M,Chakraborty D.Bearing capacity of underreamed piles in clay using lower bound finite element limit analysis[J].International Journal of Geotechnical Engineering,2022,16(9):1104–1115.

[10] Peter J A, Lakshmanan N, Manoharan P D. Investigations on the static behavior of self-compacting concrete underreamed piles[J]. Journal of Materials in Civil Engineering, 2006,18(3):408–414.

[11] Jiang Jie,Tu Xianjie,Chen Jun,et al.Prediction and numerical verification of bearing capacity of large diameter belled artificial hole digging pile[J]. Journal of Guangxi University(Natural Science Edition),2019,44(1): 132–140.[江杰,涂仙杰,陈骏,等. 大直径扩底人工挖孔桩承载力预测与数值验证[J]. 广西大学学报(自然科学版),2019,44(1): 132–140.]

[12] Zhao Liping,Long Xiaopeng,Huang Xiaoyun.Settlement analysis of composite foundation of soil-cement mixing pile[J]. Journal of Changsha University of Science and Technology(Natural Science),2020,17(3):30–36.[赵利平,龙骁鹏,黄筱云. 水泥土搅拌桩复合地基沉降分析[J]. 长沙理工大学学报(自然科学版),2020,17(3):30–36.]

[13] Mo Cheng,Yue Qidi, Liu Zhao,et al.Study on bearing capacity and mechanism of super-long and large diameter belled pile in deep soft soil area[J]. Guangdong Architecture Civil Engineering,2023,30(3):30–35.[莫成,岳琪迪,刘昭,等. 深厚软土地层超长超大直径扩底桩承载力性状及机理研究[J]. 广东土木与建筑,2023,30(3):30–35.]

[14] Cheng Hongtao,Dai Changyou, Bu Xinfeng.Characteristics of Quaternary strata in the lower reaches of the Yellow River and selection of pile foundation scheme—Taking a bridge across the Yellow River in Jinan as an example[J].Gansu Science and Technology,2022,38(18):25–28.[程红涛,代常友,卜新峰. 黄河下游第四系地层特征及桩基础方案选择——以济南某跨黄河特大桥为例[J].甘肃科技,2022,38(18):25–28.]

[15] Liu Liqun,He Qiaoling,Ma Yufei.Standard stratigraphic division and its application in municipal engineering in Jinan[J]. Urban Geotechnical Investigation & Surveying, 2022(3):196–198.[刘立群,何巧灵,马玉飞. 济南标准地层划分及其在市政工程中的应用[J]. 城市勘测,2022(3): 196–198.]

[16] Li Lianxiang, Liu Jiadian, Li Kejin, et al. Study of parameters selection and applicability of HSS model in typical stratum of Jinan[J].Rock and Soil Mechanics,2019,40(10): 4021–4029.[李连祥,刘嘉典,李克金,等. 济南典型地层HSS参数选取及适用性研究[J]. 岩土力学,2019,40(10): 4021–4029.]

[17] Dong Sansheng,Zhao Junhai,Lei Zixue.Study on the limit shaft friction resistance of long piles in the middle and lower reaches of the Huanghe River alluvial plain[J].Journal of Xi'an University of Architecture & Technology(Natural Science Edition),2011,43(4):507–512.[董三升,赵均海,雷自学. 黄河中下游冲积平原深长桩桩侧极限摩阻力研究[J]. 西安建筑科技大学学报(自然科学版),2011,43(4):507–512.]

[18] Dong Zhiqiang,Zhang Junqing,Wang Qingrong,et al. Application of precast-internal rammed immersed tube perfusion special-shaped pile in alluvial plain of lower Yellow River[C]//Thesis Collection of 2006 Academic Exchange Meeting of Architectural Structure Committee of Shandong Architectural Society and Engineering Design and Computerization Committee of Shandong Civil Engineering Society,2006:100–102.[董志强,张君卿,王青荣,等. 预制–内夯扩沉管灌注异型桩在黄河下游冲积平原的应用

[C]//山东建筑学会建筑结构专业委员会、山东土木工程学会工程设计及电算专业委员会2006年学术交流会论文集,2006:100–102.]

[19] 中华人民共和国建设部.建筑桩基技术规范:JGJ 94—2008[S].北京:中国建筑工业出版社,2008.

[20] 中华人民共和国住房和城乡建设部.建筑基桩检测技术规范:JGJ 106—2014[S].北京:中国建筑工业出版社,2014.

[21] Wang Junlin, Wang Fuming, Ren Lianwei, et al. Horizontal static load test and numerical simulation of single large diameter under-reamed pile[J]. Chinese Journal of Geotechnical Engineering,2010,32(9):1406–1411.[王俊林,王复明,任连伟,等.大直径扩底桩单桩水平静载试验与数值模拟[J].岩土工程学报,2010,32(9):1406–1411.]

[22] Zhang Zhongmiao,Xin Gongfeng,Xia Tangdai.Test and research on unrock-socketed super-long pile in deep soft soil [J].China Civil Engineering Journal,2004,37(4):64–69.[张忠苗,辛公锋,夏唐代.深厚软土非嵌岩超长桩受力性状试验研究[J].土木工程学报,2004,37(4):64–69.]

[23] Ken F, Austin W, Mark R, et al. Piling engineering[M]. 3rd ed.London:CRC Press,2014.

[24] Huang Xin,Fan Xiufeng,An Yazhou.Applicability analysis of HS model in numerical simulation of foundation pit[J]. Journal of Water Resources and Architectural Engineering, 2018,16(2):115–120.[黄鑫,樊秀峰,安亚洲.HS模型在基坑工程数值模拟中的适用性分析[J].水利与建筑工程学报,2018,16(2):115–120.]

[25] Han Jianyong,Zhao Wen,Li Tianliang,et al.Field measurement and numerical analysis of the influences between the deep excavation and adjacent buildings[J].Advanced Engineering Sciences,2020,52(4):149–156.[韩健勇,赵文,李天亮,等.深基坑与邻近建筑物相互影响的实测及数值分析[J].工程科学与技术,2020,52(4):149–156.]

[26] Ye Hongdong. Analysis and find a result about efficiency factor of bearing capacity of soil around piles in composite foundation[J].Rock and Soil Mechanics,2004,25(4): 663–665.[叶洪东.复合地基桩间土承载力折减系数的分析与取值[J].岩土力学,2004,25(4):663–665.]

[27] Wang Xiaoyang,Yang Chao,Dai Guoliang,et al.Discussion on the value of comprehensive coefficient for calculating the compression of super-long pile body in deep soft soil area[J]. Journal of China & Foreign Highway,2014,34(4): 45–48.[王晓阳,杨超,戴国亮,等.深厚软土地区超长桩桩身压缩量计算综合系数取值探讨[J].中外公路,2014, 34(4):45–48.]

[28] Qiu Rendong, Liu Jinli,Gao Wensheng, et al. Large scale model tests on settlement characteristics of long pile group foundation[J].China Civil Engineering Journal,2015,48(3): 85–95.[秋仁东,刘金砺,高文生,等.长群桩基础沉降性状的大比例尺模型试验研究[J].土木工程学报,2015,48(3): 85–95.]

[29] Hu Qinghua, Yin Yabin, Sun Jiandong, et al. Study on compression of pile in vertical compressive static load test of single pile of overlength pile[J]. Site Investigation Science and Technology,2016(4):5–8.[胡清华,殷亚斌,孙建东,等.超长桩单桩竖向抗压静载荷检测中桩身压缩量的研究[J].勘察科学技术,2016(4):5–8.]

[30] Liang Shanzhai. Field tests on vertical bearing capacity of pipe piles in cement-improved soil[J]. Chinese Journal of Geotechnical Engineering,2021,43(S2):280–283.[梁善斋.水泥土复合管桩竖向承载特性现场试验[J].岩土工程学报,2021,43(S2):280–283.]

[31] Gao Meng, Gao Guangyun, Gu Baohe, et al. Practical method for settlement calculation of large-diameter belled piles[J]. Chinese Journal of Geotechnical Engineering, 2012, 34(8): 1448–1452.[高盟,高广运,顾宝和,等.一种大直径扩底桩的沉降计算实用方法[J].岩土工程学报,2012,34(8): 1448–1452.]

[32] Chin Fung Kee.The inverse slope as a prediction of ultimate bearing capacity of piles[C]//Proceedings of 3th Southeast Asian Conference on Soil Engineering.Hong Kong:Universiti TekNologi Malaysia,1972:83–91.

[33] Van der Veen C. The bearing capacity of a pile[C]//Proceedings of the third international conference on SMFE. Switzerland:Diamond Scientific Publishing,1953:53–57.

## Study on Vertical Bearing Capacity of Rotary Drilling Variable Diameter Pile in Alluvial Formation of Lower Yellow River

*SHAO Guangbiao*[1,2], *SHEN Jiajia*[3], *JIAO Weijie*[3], *HAN Jianyong*[1,2*], *LIU Xuelin*[4], *CHEN Jiyao*[1]

(1.School of Civil Engineering, Shandong Jianzhu University, Jinan 250101, China;
2.Engineering Research Institute of Appraisal and Strengthening of Shandong Jianzhu University Co., Ltd., Jinan 250013, China;
3.Jinan International Airport Construction Co., Ltd., Jinan 250107, China;
4.China Architecture Design & Research Group, Beijing 100032, China)

**Abstract**:

**Objective** The alluvial plain in the lower reaches of the Yellow River exhibits typical sedimentary stratigraphic characteristics and is mainly composed of interbedded layers of clay, fine sand, and silty sand. Its bearing capacity is relatively low. In major infrastructure projects in this region,

rotating drilling variable-diameter piles (expanded foundation piles) demonstrate advantages in construction efficiency and settlement control. However, the vertical compressive performance and failure mechanisms of such piles under the specific geological conditions of the Yellow River alluvial layer remain insufficiently investigated. This study aims to comprehensively examine the vertical bearing capacity, load transfer characteristics, and ultimate bearing capacity of rotating drilling variable-diameter piles within this typical interbedded silty soil-clay layer, providing a theoretical and practical basis for optimizing pile design in similar geological environments.

**Methods** A series of investigations were conducted, including field experimentation, numerical simulation, and theoretical analysis. Full-scale field tests were conducted at an airport expansion site located on the Yellow River alluvial plain. Six instrumented test piles were installed using rotary drilling: three piles with a shaft diameter of 1 000 mm and three piles with a diameter of 800 mm, each featuring an enlarged base with a diameter twice that of the shaft and constructed at a precise distance above the pile tip. The piles were extensively equipped with strain gauges at multiple depths along the shaft and earth pressure cells at the base to continuously monitor internal forces and end-bearing pressures. The load tests were performed as slow maintained tests, and the piles were incrementally loaded to 1.2 times their code-calculated ultimate load to fully characterize their pre-yield and post-yield behavior and capture the complete load-settlement trajectory. Complementary three-dimensional finite element models were developed using PLAXIS 3D software to obtain insights beyond the limits of physical measurements. The complex stratified soil profile was modeled, and the constitutive model Hardening Soil was selected to simulate the mechanical behavior of the soil. The parameters used in the constitutive model were carefully calibrated and validated against the field test data to ensure model reliability. For further comparison, identical models of conventional equal-diameter piles with the same dimensions were established and subjected to the same loading and boundary conditions. In addition, a refined theoretical analytical method was applied. This method incorporated specific modifications for calculating the settlement of the enlarged base by considering its geometry and for estimating the *in-situ* soil deformation modulus from laboratory data. The proposed theoretical analytical method predicted the complete nonlinear load-settlement response and produced a more accurate back-calculation of the ultimate bearing capacity.

**Results and Discussions** The on-site tests demonstrated that the load−settlement ($Q-S$) curve of the variable-diameter pile exhibited a gradual and progressive failure mode without a distinct yield point, which was consistent with the characteristics of friction-end-bearing piles. The release of the frictional resistance and end-bearing force of the pile body did not occur simultaneously. The resistance of the upper portion of the pile body reached its limit earlier than that of the lower portion, and the complete release of the pile body's frictional resistance generally occurred before the complete release of the end-bearing force. The widened bottom section played a crucial role and contributed more than 79% to 85% of the ultimate bearing capacity of the test pile. This load distribution not only reduced the total settlement of the pile body but also effectively delayed the elastic and plastic deformation of the pile body itself. Therefore, it provided more favorable conditions for the gradual mobilization of lateral resistance of the pile body in deeper and stiffer strata compared to straight piles. In cases of premature failure, these lateral resistances will not have been fully mobilized. In addition, compared to straight piles, the ratio of elastic compression of the pile body to the total settlement at the pile top of the variable-diameter pile was significantly lower, which indicated that its structural load transfer more closely followed general mechanical behavior. The analysis of the relative displacement between the pile and the soil showed that sliding initiated in the upper soil layer and gradually expanded downward as the load increased until it extended to the expansion base area under the ultimate load. The presence of the enlarged base prevented sudden failure of the pile body. The numerical simulation results confirmed the experimental observations. The ultimate bearing capacity of the variable-diameter pile obtained from the calibrated model was approximately 10% higher than that of the geometrically equivalent straight pile. The evolution of the plastic zone in the surrounding soil differed significantly: for the variable-diameter pile, the plastic yielding phenomenon initiated simultaneously near the pile head and in the expansion base area and then expanded downward from the top. During the failure process, the lateral extent remained within approximately 2 meters around the pile body. In contrast, for straight piles, the plastic zone expanded more extensively in both vertical and horizontal directions and frequently extended to the model boundary under the ultimate load, indicating a broader range of soil failure. The analysis of settlement influence showed that the surface settlement caused by the variable-diameter pile was significantly smaller than that produced by the straight pile and remained more localized. Through theoretical calculations, a predicted load−settlement curve that was highly consistent with the measured data was obtained, with errors typically ranging from 6% to 15%. Using this method, the ultimate bearing capacity obtained from the back-calculation agreed well with the numerical simulation results and the maximum test load. This agreement indicated that, within this stratum, the actual ultimate bearing capacity of the variable-diameter pile was approximately 10% to 20% higher than the value calculated using the empirical formula in the current Chinese standard (JGJ 94—2008).

**Conclusions** In the alluvial layer of the lower reaches of the Yellow River, the rotating drilling variable-diameter pile behaves as a typical friction end-bearing pile. The release of pile body resistance does not occur simultaneously but instead proceeds segment by segment along the pile depth direction. Specifically, the upper part first releases its resistance completely, after which the lower part begins to release its resistance. The en-

larged pile bottom significantly enhances the end-bearing effect, reduces and delays settlement, and raises a more complete release of the pile body frictional resistance, improving the overall vertical bearing capacity. Compared to the straight column-type pile, the pile body compression of the variable-diameter pile is relatively smaller, and the total settlement is also reduced. Its performance more closely resembles that of a non-rigid pile and produces a more localized influence on the surrounding soil. Its failure mechanism is characterized by the simultaneous formation of plastic zones at the pile head and the enlarged pile bottom. During loading, the plastic zone gradually expands from the top toward the bottom. In the ultimate state, the failure process is progressive, and the significant plastic deformation of the surrounding soil is limited to the area within approximately 2 meters from the pile body. This behavior differs from the extensive failure zone typically observed in straight piles. Under these specific geological conditions, the actual ultimate bearing capacity of this variable diameter pile is approximately 10% to 20% higher than the value calculated using current standard normative methods. The combination of on-site testing, numerical simulation, and revised theoretical analysis provides a reference for evaluating and predicting the performance of such piles.

**Key words**: the Yellow River alluvial formation; variable diameter pile; static load test; stress performance; ultimate bearing capacity; numerical simulation

（编辑　李轶楠）

**引用格式**: Shao Guangbiao,Shen Jiajia,Jiao Weijie,et al.Study on vertical bearing capacity of rotary drilling variable diameter pile in alluvial formation of lower yellow river[J].Advanced Engineering Sciences,2026,58(2):179–190.[邵广彪,申佳佳,焦伟杰,等.黄河下游冲积地层旋挖变径桩竖向承载性能研究[J].工程科学与技术,2026,58(2):179–190.]